Tetrahedron 67 (2011) 1238–1244

Contents lists available at ScienceDirect

Tetrahedron

journal homepage: www.elsevier.com/locate/tet

From smectic to columnar phase of polypedal liquid crystals based on tetrathiafulvalene/1,3-dithiol-2-thione and cholesterol

Ruibin Hou [a], Ke-li Zhong [a], Zhegang Huang [b], Long Yi Jin [a,*], Bingzhu Yin [a,*]

[a] Key Laboratory of Natural Resources of Changbai Mountain & Functional Molecules, Yanbian University, Ministry of Education, Yanji, Jilin 133002, PR China
[b] Center for Supramolecular Nano-Assembly and Department of Chemistry, Seoul National University, 599 Kwanak-ro, Seoul 151-747, South Korea

ARTICLE INFO

Article history:
Received 19 August 2010
Received in revised form 8 November 2010
Accepted 26 November 2010
Available online 1 December 2010

Keywords:
Polypedal liquid crystals
Tetrathiafulvalene
Cholesterol
Glassy mesogen
Smectic phase
Hexagonal columnar phase

ABSTRACT

Bipedal 1,3-dithiole-2-thiones attached two cholesteryl through a ω-thioalkanoyloxy spacer of varying length were synthesized. The bipedals were easily transformed to the appropriate tetrapedal tetrathiafulvalene derivatives by self-coupling reaction in net triethyl phosphite. All the synthesized compounds exhibit mesogenic phases in a wide temperature region, no crystallization but vitrifying to form glassy mesogens during cooling from the isotropic melt. The liquid crystals with shorter spacer (n=2–6) exhibited only a smectic A phase and those with the longest spacer (n=7) exhibited only a hexagonal columnar. In these series, the molecular packing depended on the length of spacers.

1. Introduction

Recently a lot of efforts have been made to basic and applied studies on ordered molecular organizations formed by relatively weak intermolecular interactions, such as liquid crystals, organogels, and Langmuir–Blodgett (LB) films, because they show new optical or electrical properties, which were not observed in the single molecule.[1–3] Since weak interactions are sensitively influenced by external stimuli, such as light, temperature, and electric field, properties of these molecules can be easily controlled.[4] In developing novel organic materials, liquid crystals (LCs) are currently viewed as highly potential candidate because the mesophases offer soft phases with lamellar, columnar or cubic arrangements, and a current goal is to use the fourth state of matter to achieve ordered functional systems.[5,6]

Tetrathiafulvalene (TTF) derivatives have played a pivotal role in the development of organic materials for optoelectronic application due to their excellent electron-donating properties.[7–9] The transport properties of these materials are clearly dependent on the molecular architecture in the solid state and so a wide variety of substituents have been introduced at the periphery of the TTF core in order to achieve a suitable solid-state organization.[10] In this respect, a possible approach is based on the preparation of mesogenic compounds. In particular, glassy liquid crystals (GLCs) hold a fast and good orientation, which can be readily processed into macroscopically ordered solid films.[11] However, most researches into TTF and its derivatives have been focused on their crystalline phase. Although a considerable number of TTF derivatives have so far been synthesized, there are only a few reports describing TTF derivatives with mesomorphic properties[12–20] and consequently, it is not yet possible to establish structure–property relationships for this family of compounds.

In order to study the effect of structure on the possible liquid crystal behavior of new TTF derivatives, we selected cholesteryl as side group, which has been successfully used in the preparation of chiral liquid crystals, and introduced it to the periphery of TTF unit through flexible spacers. Here, we report the synthesis and mesomorphic properties of TTF-based tetrapedals **1a**–**f** containing four cholesteryls and 1,3-dithiol-2-thione-baesd bipedals **4a**–**f** containing two cholesteryls, together with the electron donating property of tetrapedals **1a**–**f** with a TTF central core. Compounds **4f** and **1f** with the longest spacer showed a hexagonal columnar phase (Col_h) at a wide and low temperature region. The tetrapedal **1f** with a TTF central core showing a Col_h mesophase in a wide temperature range is reported for the first time to our knowledge although there is only one report of Col_h mesogenic compound based on TTF, which is short of X-ray diffraction data to confirm the Col_h structure.[21]

* Corresponding authors. Tel.: +86 433 2732298; fax: +86 433 2732456; e-mail addresses: lyjin@ybu.edu.cn (L.Y. Jin), zqcong@ybu.edu.cn (B. Yin).

0040-4020/$ – see front matter © 2010 Elsevier Ltd. All rights reserved.
doi:10.1016/j.tet.2010.11.088

2. Results and discussion

UV–vis spectra were recorded on a Hitachi U-3010 spectrophotometer in CH_2Cl_2 ($c=1\times10^{-5}$ M). Cyclic voltammetric studies were carried out on a Potentiostat/Galvanostat 273A instrument in CH_2Cl_2 ($c=1\times10^{-3}$ M) and 0.1 M Bu_4PF_6 as the supporting electrolyte. Counter and Working electrodes were made of Pt and Glass–Carbon, respectively, and the reference electrode was calomel electrode (SCE). A Perkin–Elmer Pyris Diamond differential scanning calorimeter was used to determine the thermal transitions, which were reported as the maxima and minima of their endothermic or exothermic peaks, the heating and cooling rates were controlled to 10 °C/min. An Olympus BX51-P optical polarized microscope (magnification: 40×), equipped with a Mettler FP82 hot-stage and a Mettler FP90 central processor, was used to observe the thermal transitions and to analyze the anisotropic texture. The thermal stability of target compounds were characterized by Shimadzu DTG-60H thermogravimetric analyzer. X-ray scattering measurements were performed in transmission mode with synchrotron radiation at the 3C2 X-ray beam line at Pohang Accelerator Laboratory, Korea.

2.1. Synthesis

The structures and synthetic route of target tetrapedals were shown in Scheme 1. The reaction of bis(tetraethylammonium) bis (1,3-dithiole-2-thione-4,5-dithiol) zincate salt (**2**) with cholesteryl ω-bromoalkyanoates (**3**) in acetonitrile gave bipedal 1,3-dithiol-2-thione derivatives **4** in good yields (70–78%), and phosphite-mediated self-coupling of **4** eventually obtained the desired tetrapedal liquid crystal compounds **1a**–**f** (41–47%).

(n=5) exhibited a liquid crystalline phase at a melting state (17.7 °C), which was transformed to an isotropic phase at 97.4 °C (Fig. 1a and Table 1). On slow cooling of **4d** from the isotropic liquid to liquid crystalline phase, a banded focal conic fan texture was observed by POM experiment, which was transformed to glassy state during cooling (Fig. 2a). The DSC curves together with optical texture preliminarily confirmed the presence of a 1-D smectic A phase (S_A). The SAXS of **4d** measured at cooling to 80 °C displayed three sharp reflections with d spacings of 4.95, 2.47, and 1.65 nm, which were in the ratio of 3:2:1 and agreed well with (100), (200), and (300) reflections of a lamellar packing structure (Fig. 3a). Considering the layer thickness (4.95 nm) obtained from the X-ray diffraction pattern is much larger than the estimated molecular length (2.5 nm by Corey–Pauling–Koltun (CPK) model) and the S···S interaction between the 1,3-dithiole-2-thione segments, bimolecule arrangement in lamellar structure is expected, in which the 1,3-dithiole-2-thione segments interdigitate to fill the space (Fig. 4a). The small-angle X-ray diffraction pattern of **4b** (n=3) also displayed similar Bragg diffraction peaks corresponding to the long spacing or layer reflections in the small-angle region (Table 2 and Fig. S4) and thus also index to a lamellar structure. Considering the similarity of the optical textures with those of **4b** and **4d**, **4a**, **4c**, and **4e** could also be indexed to lamellar arrangement (Fig. S2). The compound **4f** (n=7) with the longest spacer is unique in that it displays two mesophases at 10.7 °C and 77.5 °C, followed by transformation to an isotropic phase at 89.2 °C (Table 1 and Fig. 1b). Upon cooling from the isotropic liquid, a cholesteric-like texture was observed by POM experiment (Fig. 2b). The DSC curves together with optical texture preliminarily considered to be a cholesteric phase. To identify the detailed phase structure, SAXS studies were performed. The X-ray diffractogram of **4f** taken at 85 °C shows

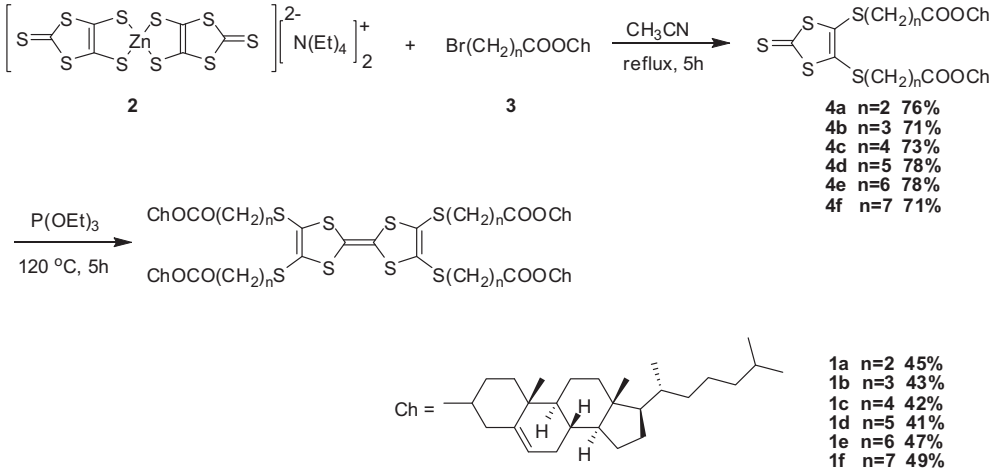

Scheme 1. The synthetic route of **1a**–**1f**.

2.2. Characterization of liquid crystal phase

The phase sequences and phase structures of key precursor bipedals **4a**–**f** and target tetrapedals **1a**–**f** were investigated by polarized-light optical microscopy (POM), differential scanning calorimetry (DSC), and small-angle X-ray scatterings (SAXS). All the synthesized compounds exhibit mesophases and no crystallization but vitrifying to form glassy mesogen during cooling from the isotropic melt. The bipedals **4a**–**e** exhibited only one mesophase in a wide temperature region. Only compound **4f** with the longest spacer showed two phase transitions in heating as well as in cooling cycle (Table 1, Fig. 1 and Fig. S1). For example, compound **4d** a strong diffuse halo in the wide-angle X-ray regions, but no sharp peak in the lower Bragg angle region was observed, indicating the presence of a cholesteric phase (Fig. 3b). On further cooling to 75.5 °C, the cholesteric phase gradually transformed to another mesophase, the typical fine mosaic texture appeared and its disordered systems induce vitrification rather than crystallization during cooling (Table 1, Figs. 1b and 2c). The detailed mesophase structure is also confirmed by SAXS experiments. The X-ray diffraction pattern of **4f** measured at cooling to 60 °C displays three sharp reflections corresponding to spacing of 5.01, 2.85, and 1.87 nm in the small-angle region as shown in Fig. 3c. They are in the ratio of 1:√3:√7 and could be indexed as (100), (110), and (210)

Table 1
Phase transition temperature and enthalpy changes of **4a**–**f** and **1a**–**f** determined by DSC in the second cooling scan[a]

Compd	Transition temperature (°C) and enthalpy changes (J g^{-1}), Heating cycle/Cooling cycle	ΔT[b]/°C	T_d[c]/°C
4a	g 38.3 (0.6) S_A 133.1 (2.7) I/I 128.8 (2.7) S_A 36.3 g	94.8	
4b	g 31.1 (0.5) S_A 104.6 (4.5) I/I 134.6 (7.1) S_A 28.4 g	106.4	
4c	g 22.4 (0.7) S_A 104.6 (4.5) I/I 102.4 (4.2) S_A 20.8 g	82.2	
4d	g 17.7 (0.9) S_A 97.4 (4.7) I/I 95.4 (4.7) S_A 15.3 g	79.7	
4e	g 11.2 (0.9) S_A 80.1 (3.6) I/I 77.3 (3.6) S_A 9.6 g	68.9	
4f	g 10.7 (0.8) Col_h 77.5 (1.7) Ch 89.2 (0.5) I/ I 87.1 (0.7) Ch 75.7 (1.7) Col_h 8.3 g	66.8; 11.7	
1a[d]	Cr 200.5 (57.7) I/I 159.0 (3.4) S_A—g	—	295
1b	g 57.8 (0.3) S_A 148.5 (2.7) I/I 145.5 (2.6) S_A 54.7 g	90.7	296
1c	g 50.3 (0.4) S_A 136.5 (3.8) I/I 133.2 (3.7) S_A 45.8 g	86.2	298
1d	g 48.7 (1.4) S_A 130.8 (4.2) I/I 127.4 (4.1) S_A 43.3 g	82.1	303
1e	g 37.1 (0.7) S_A 120.9 (4.3) I/I 116.5 (4.3) S_A 35.1 g	83.8	305
1f	g 34.4 (0.6) Col_h 114.8 (4.9) I/I 111.7 (3.7) Col_h 31.6 g	80.4	308

[a] g=glass state, S_A=smectic A, Col_h=hexagonal columnar, Ch=cholesteric, I=isotropic.
[b] Mesophase temperature ranges on heating cycle.
[c] Temperature at which 5% weight loss occurred.
[d] Monotropic mesogen.

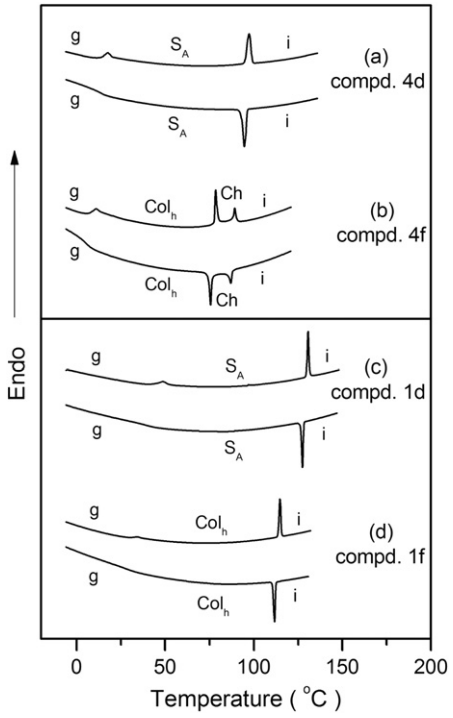

Fig. 1. DSC traces (10 °C/min) recorded during the second heating and the second cooling scan of compounds **4d**, **4f**, **1d**, **1f**.

planes of a 2-D hexagonal columnar structure with a lattice constant of 5.72 nm. Considering the lattice constant and extended molecular length (3.0 nm by CPK model). From the experimental values of the unit cell parameters (a, b, c, and γ) and the density (ρ),[22,23] the average number of molecules per cross-sectional slice of the column can be calculated according to Eq 1, where M

$$n = abc\rho N_A \sin\gamma / M \quad (1)$$

is the molecular mass and N_A is Avogadro's number. The average number (n) of molecules in each bundle of **4f** is calculated to be about 8. Obviously, the sixteen cholesteryls in a wedge shaped molecule can effectively surround the hexagonal lattice and a nearly circular shape of the columns can be assumed.[22] On the basis of the data, the schematic representation of the hexagonal columnar structure of **4f** can be illustrated as shown in Fig. 4a.

All of the target tetrapedals **1a**–**f** exhibited only one mesophase in a wide temperature region and vitrifyied to from glassy mesogens with an above-ambient glass transition temperature (T_g) during cooling process (Table 1). Meanwhile, the thermogravimetric analysis (TGA) results showed that temperatures were higher than 295 °C when 5% weight loss occurred (T_d), which revealed that the target compounds had a high thermal stability (Table 1). The small-angle X-ray diffraction patterns of **1a**–**e**, which have shorter spacers (n=2–6), displayed several sharp reflections, which correspond to equidistant q-spacings (Table 2, Fig. 3c, and Fig. S4) and thus can be indexed to the lamellar lattices. For example, compound **1d** exhibits a birefringent liquid crystalline phase at a melting state (48.7 °C), followed by transformation to an isotropic phase at 130.8 °C (Fig. 1c). On slow cooling of the isotropic liquid to 110 °C, a banded focal conic fan texture was observed by POM experiment (Fig. 2d), which vitrifying to from glassy state upon further cooling. The SAXS of **1d** measured at cooling to 90 °C displayed three sharp reflections corresponding to spacing of 4.85, 2.44, and 1.62 nm, which were in the ratio of 3:2:1, and agreed well with (100), (200), and (300) reflections of lamellar packing structure (Fig. 3d). The obtained molecular length of **1d** was 4.85 nm, which was very close to the corresponding estimated molecular length (4.5 nm by CPK model), indicative of a mono-molecule layer structure (Fig. 4b). One noteworthy point is that TTF-based tetrapedal **1f** (n=7) with the longest spacer exhibited a columnar mesophase in a considerably wide temperature window between 34.4 and 114.8 °C (Fig. 1d), which preliminarily assigned as hexagonal columnar phase from fine mosaic texture observed by microscopy (Fig. 2e). The detailed mesophase structure of **1f** was also confirmed by X-ray scattering experiments. The X-ray diffraction pattern of **1f** at 80 °C showed a diffuse halo at 0.53 nm in the wide-angle region and three sharp reflections corresponding to spacing of 4.74, 2.76, and 1.80 nm in the small-angle region as shown in Fig. 3e. They were in the ratio of 1:$\sqrt{3}$:$\sqrt{7}$ and could be indexed as (100), (110), and (210) planes of a 2-D hexagonal columnar structure. From the observed d spacing of the (100) reflection, the column diameter was calculated to be 5.50 nm, which was close to the corresponding estimated molecular length (5.2 nm by CPK model). The number of molecules in a disk was calculated to be nearly 4 by Eq 1 and the schematic representation of the hexagonal columnar structure characterized by POM and SAXS can be illustrated as shown in Fig. 4b. Similar to triblock coil–rod–coil systems,[24] the

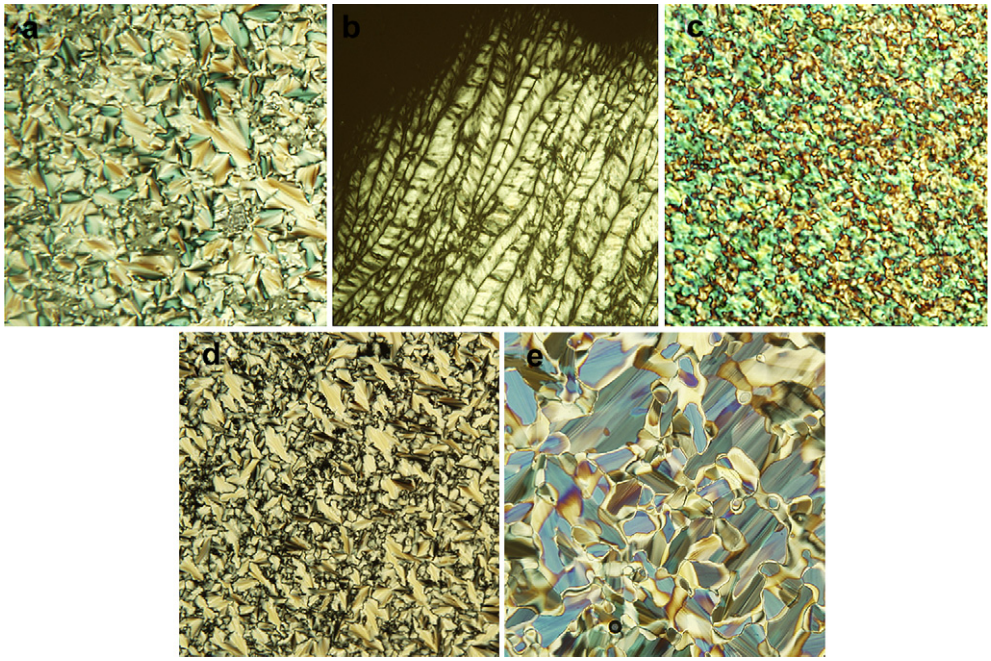

Fig. 2. Optical polarized micrographs (40×) of the texture exhibited by (a) the S_A phase of **4d** at 80 °C; (b) The Ch phase of **4f** at 80 °C; (c) The Col_h phase of **4f** at 60 °C; (d) The S_A phase of **1d** at 110 °C; (e) The Col_h phase of **1f** at 80 °C.

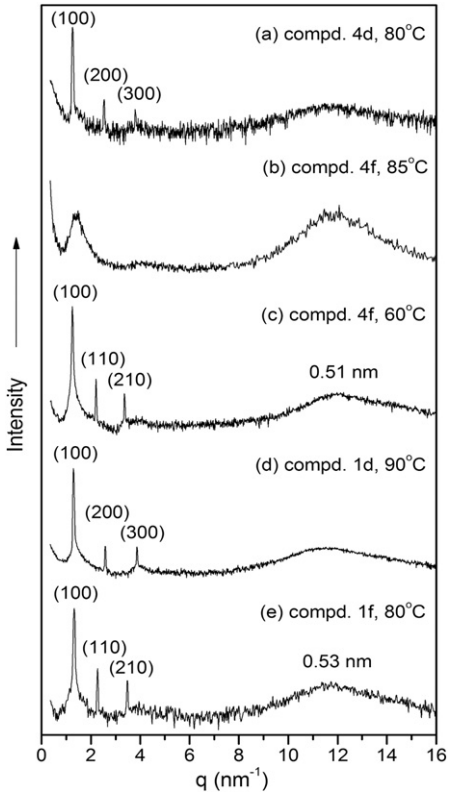

Fig. 3. X-ray diffraction patterns of **4d**, **4f**, **1d**, and **1f** plotted against $q=4\pi \sin\theta/\lambda$ measured at different temperature. (a) the S_A phase of **4d**, (b) the Ch phase of **4f**, (c) the Col_h phase of **4f**, (d) the S_A phase of **1d**, (e) the Col_h phase of **1f**.

molecular packing in the present two series depends on the length of spacers, increasing the volume fraction of flexible segments induces a hexagonal columnar mesophase. The shorter spacer is unfavorable to a columnar structure packing because it probably produces a smaller disk to induce the crowding between cholesteryl groups.

2.3. Electron donating property of target compounds

To evaluate electron donating property of target compounds, the cyclic voltammetry (CV) measurements were performed in a dry dichloromethane solution of Bu_4NBF_4 (0.1 M) with a scan rate of 100 mV s^{-1} at room temperature (Table 3). TTF-based tetrapedals **1a**–**f** showed two reversible single-electron oxidation peaks at ~0.60 and ~0.94 V, corresponding to the formation of radical cations and dications of TTF, respectively, indicating two sequential reversible one-electron transfer steps (Fig. S5). The oxidation potentials of **1a**–**f** were higher than those of 2,3,6,7-tetrakis (methylthio) tetrathiafulvalene (TMT-TTF) probably due to the existence of electron-withdrawing ester linkages in the distance. Therefore, as the methylene spacer lengthened (from n=2 to n=7), the half-wave potential was anodic shifted in a regular manner.

To investigate the potential of these structures to act as a conducting architecture, chemical oxidation of **1f** in dichloromethane solution (10^{-5} M) was conducted with stepwise addition of 7,7,8,8-tetracyanoquinodimethane (TCNQ). But no charge transfer (CT) absorption was observed in the 600–1000 nm region. Whereas, upon addition of 1 equiv of 2,3,5,6-tetrafluoro-7,7,8,8-tetracyanoquinodimethane (F_4TCNQ) to a CH_2Cl_2 solution of **1f** (10^{-5} M) resulted in the appearance of two new CT absorption bands, centered on 748 nm and 847 nm in the UV–vis spectrum (Fig. S6). These new bands correspond to the SOMO–LUMO transition of the cation radical species of the TTF moieties.[25,26] The formation of a F_4TCNQ^-/TTF^+ charge transfer complex was also confirmed by the FT-IR spectrum. The FT-IR spectrum of the complex showed the nitrile stretch of the F_4TCNQ radical anion at 2193 cm^{-1} compared to the neutral state of 2222 cm^{-1} (Fig. S7).[27] Furthermore, when stepwise addition of I_2 (1→7 equiv) to a CH_2Cl_2 solutions of **1f**, two new CT absorption bands at 498 and 854 nm appeared (Fig. 5). The absorptions at 498 nm could be assigned to an intermolecular electron transfer of radical cation of **1f**, while the absorption band

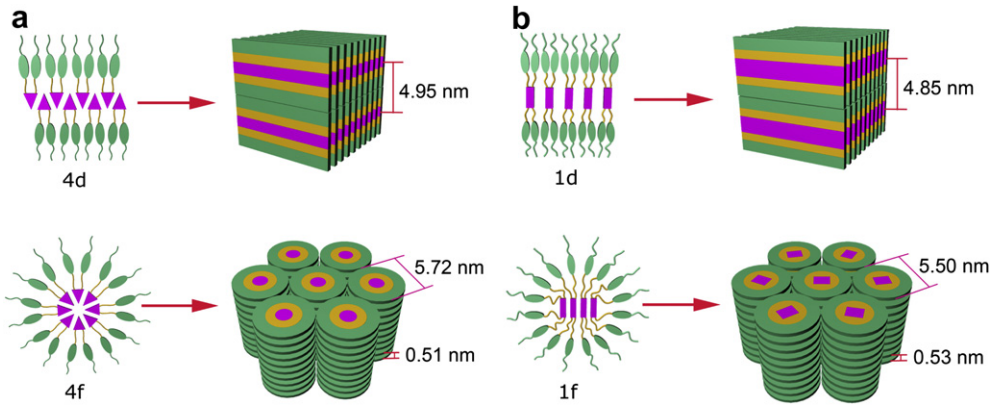

Fig. 4. Schematic representation for (a) the smectic phase of **4d** and the hexagonal columnar phase of **4f**, (b) the smectic phase of **1d** and the hexagonal columnar phase of **1f**.

Table 2
X-ray data for the selected compounds

Compd	Measured spacing/nm
4b	4.49 (100), 2.24 (200), 1.50 (300)
4d	4.95 (100), 2.47 (200), 1.65 (300)
4f	5.01 (100), 2.85 (110), 1.87 (210)
	a=b=5.72 nm, c=0.51 nm
1a	4.24 (100), 2.12 (200), 1.42 (300)
1b	4.46 (100), 2.24 (200), 1.49 (300)
1c	4.60 (100), 2.31 (200), 1.55 (300)
1d	4.85 (100), 2.44 (200), 1.62 (300)
1e	4.91 (100), 2.52 (200), 1.67 (300)
1f	4.74 (100), 2.76 (110), 1.80 (210)
	a=b=5.50 nm, c=0.53 nm

a, b, c: lattice parameters.

Table 3
Half-wave potentials of **1a**–**f** versus SCE in CH_2Cl_2 (10^{-3} M)

Compd	$E^1_{1/2}$/V	ΔE^1	$E^2_{1/2}$/V	ΔE^1
TMT-TTF	0.499	0.108	0.802	0.111
1a	0.597	0.122	0.939	0.118
1b	0.561	0.151	0.915	0.154
1c	0.521	0.103	0.867	0.106
1d	0.518	0.116	0.869	0.118
1e	0.514	0.138	0.868	0.136
1f	0.511	0.158	0.865	0.165

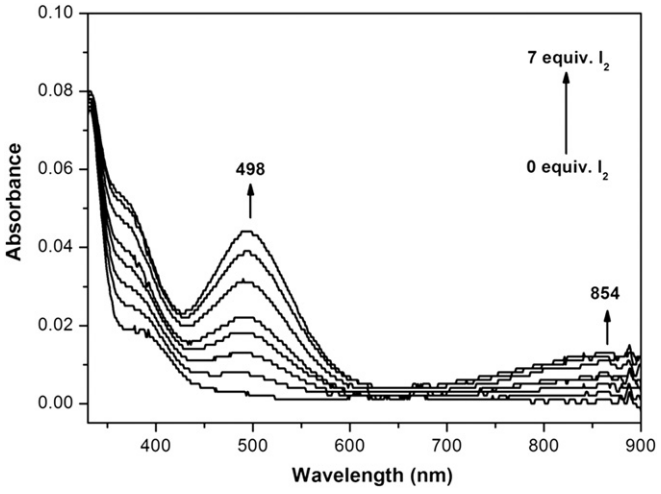

Fig. 5. UV–vis absorption spectral change of **1f** (1×10^{-5} M) in CH_2Cl_2 solutions upon stepwise addition of I_2.

at 854 nm was due to an intermolecular electron transfer of the π-dimer of **1f** dications.[28]

3. Conclusions

We have synthesized two novel series of polypedal liquid crystals based on TTF/dithiole-2-thione and cholesterols. polypedals **4a**–**e** and **1a**–**e** with shorter spacer (n=2–6) showed only one smectic A mesophase in a wide temperature region, whereas **4f** and **1f** with the longest spacer (n=7) exhibited a hexagonal columnar phase. All of polypedals formed glassy mesogens with an above-ambient glass transition temperature during cooling from the isotropic melt. From smectic to columnar phase change of these series are entirely dependent on the length of spacer, increasing the volume fraction of flexible segments induces a hexagonal columnar phase. TTF-based tetrapedal liquid crystals **1a**–**f** exhibited good electron-donating properties. These liquid crystals, in combination with high thermal stability and the inherent optoelectronic properties of TTF, may provide new opportunities in the development of ordered soft materials.

4. Experimental

4.1. General

NMR spectra were recorded in $CDCl_3$ with a Bruker AV-300 Spectrometer (300 MHz for ^{1}H and 75 MHz for ^{13}C) and chemical shifts were referenced relative to tetramethylsilane (δ_H/δ_C=0). IR spectra were recorded on a Shimadzu FT-IR Prestige-21 instrument (KBr pressed disc method). MALDI-TOF-MS was performed on a Shimadzu Axima CFR™ *Plus* using a 1,8,9-anthracenetriol (DITH) matrix. Compounds **2** and **3** were synthesized according to our literature method.[29,30]

4.2. Typical procedure for compound 4f

To a solution of bis(tetraethylammonium) bis (2-thioxo-1,3-dithiole-4,5-dithiolato) zincate (1.0 g, 1.4 mmol) in dry MeCN (20 ml) was added compound **1** (3.31 g, 5.6 mmol) and the mixture was refluxed for 5 h. The resulting precipitate was filtered off and the brownish yellow filtrate was concentrated in vacuo. The residue was dissolved in CH_2Cl_2 (25 ml) and washed with H_2O (3×20 ml), dried on $MgSO_4$. After evaporation of the solvent in vacuo, yellow oily residue was obtained, which was purified by column chromatography (silica gel, CH_2Cl_2) to give **4f** as a yellow slimy solid 1.22 g (yield: 71.2%). ^{1}H NMR ($CDCl_3$): δ 0.68–2.40 (108H, m, aliphatic and cholesteric protons are overlapped), 2.86 (6H, t, J 7.2 Hz, SCH_2), 4.50–4.72 (2H, m, OCH), 5.35–5.39 (2H, m, =CH). ^{13}C NMR

($CDCl_3$, 75 MHz): δ 11.86, 18.74, 19.33, 21.05, 22.59, 22.83, 23.86, 24.29, 24.88, 27.83, 27.99, 28.24, 28.30, 28.71, 28.91, 29.57, 31.86, 31.90, 34.54, 35.79, 36.20, 36.58, 36.68, 37.01, 38.17, 39.52, 39.74, 42.30, 50.03, 56.16, 56.68, 73.69, 122.58, 136.19, 139.64, 172.95, 211.09. FT-IR (KBr, cm^{-1}): 1734 (C=O). Anal. Calcd for $C_{73}H_{118}O_4S_5$: C, 71.86; H, 9.75. Found: C, 71.63; H, 10.01.

4.2.1. Compound ***4a***. Yellow slimy solid, yield: 76%. ^1H NMR ($CDCl_3$): δ 0.68–2.34 (86H, m, aliphatic and cholesteric protons are overlapped), 2.67 (4H, t, *J* 7.0 Hz, $COCH_2$), 3.12 (4H, t, *J* 7.0 Hz, SCH_2), 4.55–4.76 (2H, m, OCH), 5.37–5.39 (2H, m, =CH). ^{13}C NMR (75 MHz, $CDCl_3$): δ 11.86, 18.74, 19.31, 21.04, 22.58, 22.83, 23.86, 24.28, 27.77, 28.23, 30.33, 31.71, 31.834, 31.90, 34.22, 34.83, 35.80, 36.57, 36.96, 38.08, 39.52, 39.73, 42.31, 50.01, 56.16, 56.68, 74.87, 122.90, 136.67, 139.39, 170.12, 210.71. FT-IR (KBr, cm^{-1}): 2945 (C–H), 1732 (C=O), 1074 (C–O). Anal. Calcd for $C_{63}H_{98}O_4S_5$: C, 70.08; H, 9.15. Found: C, 70.40; H, 8.91.

4.2.2. Compound ***4b***. Yellow slimy solid, yield: 71%. ^1H NMR ($CDCl_3$): δ 0.68–2.33 (90H, m, aliphatic and cholesteric protons are overlapped), 2.46 (4H, t, *J* 7.1 Hz, $COCH_2$), 2.94 (4H, t, *J* 7.1 Hz, SCH_2), 4.47–4.78 (2H, m, OCH), 5.38–5.40 (2H, m, =CH). ^{13}C NMR (75 MHz, $CDCl_3$): δ 11.86, 18.74, 19.31, 21.05, 22.56, 22.80, 23.86, 24.28, 24.95, 27.83, 27.98, 28.21, 31.86, 31.90, 32.84, 35.78, 36.00, 36.20, 36.58, 37.00, 38.15, 39.52, 39.75, 42.31, 50.05, 56.20, 56.70, 74.27, 122.73, 136.22, 139.50, 171.64, 210.70. FT-IR (KBr, cm^{-1}): 2945 (C–H), 1728 (C=O), 1067 (C–O). Anal. Calcd for $C_{65}H_{102}O_4S_5$: C, 70.47; H, 9.28. Found: C, 70.12; H, 9.30.

4.2.3. Compound ***4c***. Yellow slimy solid, yield: 73%. ^1H NMR ($CDCl_3$): δ 0.69–2.33 (98H, m, aliphatic and cholesteric protons are overlapped), 2.90 (4H, t, *J* 6.8 Hz, SCH_2), 4.55–4.66 (2H, m, OCH), 5.38–5.42 (2H, m, =CH). ^{13}C NMR (75 MHz, $CDCl_3$): δ 11.86, 18.72, 19.32, 21.04, 22.56, 22.81, 23.84, 24.28, 27.84, 27.99, 28.22, 29.03, 31.86, 31.90, 33.91, 35.78, 36.19, 36.31, 36.59, 37.00, 38.16, 39.51, 39.74, 42.31, 50.03, 56.17, 56.69, 74.03, 122.70, 136.16, 139.56, 172.34, 210.95. FT-IR (KBr, cm^{-1}): 2945 (C–H), 1730 (C=O), 1067 (C–O). Anal. Calcd for $C_{67}H_{106}O_4S_5$: C, 70.85; H, 9.41. Found: C, 70.56; H, 9.14.

4.2.4. Compound ***4d***. Yellow slimy solid, yield: 78%. ^1H NMR ($CDCl_3$): δ 0.68–2.40 (102H, m, aliphatic and cholesteric protons are overlapped), 2.87 (4H, t, *J* 7.2 Hz, SCH_2), 4.45–4.68 (2H, m, OCH), 5.36–5,40 (2H, m, =CH). ^{13}C NMR (75 MHz, $CDCl_3$): δ 11.86, 18.73, 19.31, 21.04, 22.55, 22.79, 23.85, 24.27, 24.41, 27.84, 27.91, 27.97, 28.20, 29.30, 31.88, 34.34, 35.77, 36.20, 36.50, 36.59, 37.01, 38.17, 39.51, 39.75, 42.31, 50.06, 56.19, 56.70, 73.86, 122.61, 136.15, 139.63, 172.61, 210.99. FT-IR (KBr, cm^{-1}): 2936 (C–H), 1732 (C=O), 1067 (C–O). Anal. Calcd for $C_{69}H_{110}O_4S_5$: C, 71.20; H, 9.53. Found: C, 70.98; H, 9.66.

4.2.5. Compound ***4e***. Yellow slimy solid, yield: 78%. ^1H NMR ($CDCl_3$): δ 0.68–2.32 (106H, m, aliphatic and cholesteric protons are overlapped), 2.87 (4H, t, *J* 7.2 Hz, SCH_2), 4.45–4.68 (2H, m, OCH), 5.386–5.38 (2H, m, =CH). ^{13}C NMR (75 MHz, $CDCl_3$): δ 11.84, 18.72, 19.29, 22.53, 22.76, 23.84, 24.26, 24.77, 27.95, 28.11, 28.16 , 28.48, 29.40 , 31.89, 34.45, 35.75, 36.13, 36.20, 36.61, 37.01, 38.18, 39.51, 39.75, 42.31, 50.07, 56.20, 56.70, 73.77, 122.57, 136.17, 139.64, 172.80, 211.08. FT-IR (KBr, cm^{-1}): 2936 (C–H), 1730 (C=O), 1067 (C–O). Anal. Calcd for $C_{71}H_{114}O_4S_5$: C, 71.54; H, 9.64. Found: C, 71.86; H, 9.89.

4.3. Typical procedure for compounds 1a–f

Compound **4f** (3.99 g, 3.27 mmol) was added to $P(OEt)_3$ (50 mL) and the suspension was heated to 120 °C, causing dissolution within 1 min, leaving a yellow reaction mixture. The mixture was stirred for 5 h at 120 °C, cooled to room temperature. Addition of MeOH (50 mL) gave a yellow solid, which was filtered, washed with MeOH, and dried in vacuo. The products were purified by column chromatography (silica gel, CH_2Cl_2) to give a yellow solid. The solid was recrystallized from acetone–THF gave **1f** as a orange powder (yield: 49%). ^1H NMR ($CDCl_3$, 300 MHz): δ 0.68–2.24 (220H, m, aliphatic and cholesteric protons are overlapped), 2.81 (8H, t, *J* 7.2 Hz, SCH_2), 4.50–4.69 (4H, m, OCH), 5.34–5.37 (4H, m, =CH). ^{13}C NMR ($CDCl_3$, 75 MHz): δ 11.35, 18.72, 19.33, 21.03, 22.56, 22.81, 23.84, 24.94, 27.83, 28.01, 28.23, 28.76, 28.97, 29.64, 31.86, 35.79, 36.19, 38.17, 39.52, 39.74, 42.31, 50.03, 56.15, 56.69, 73.72, 122.60, 127.72, 139.69, 173.13. IR (KBr, cm^{-1}): 2931 (C–H), 1734 (C=O), 1171 (C–O). MS (MALDI-TOF): *m*/*z* 2374.4073 [M^+, 100%]. Anal. Calcd for $C_{146}H_{236}O_8S_8$: C, 73.80; H, 10.01. Found: C, 73.68; H, 9.93.

4.3.1. Compound ***1a***. Orange powder, yield: 45%. ^1H NMR ($CDCl_3$, 300 MHz): δ 0.68–2.34 (172H, m, aliphatic and cholesteric protons are overlapped), 2.68 (8H, t, *J* 7.0 Hz, $COCH_2$), 3.06 (8H, t, *J* 7.0 Hz, SCH_2), 4.51–4.74 (4H, m, OCH), 5.36–5.40 (4H, m, =CH). ^{13}C NMR ($CDCl_3$, 75 MHz): δ 11.87, 18.73, 19.33, 21.05, 22.56, 22.81, 23.87, 24.29, 27.79, 28.01, 28.23, 31.18, 31.86, 31.96, 35.06, 35.81, 36.20, 36.99, 38.11, 39.52, 39.75, 42.32, 50.03, 56.18, 56.70, 74.64, 122.79, 128.32, 139.52, 170.52. FT-IR (KBr pellet, cm^{-1}): 2945 (C–H), 1734 (C=O), 1184 (C–O). MS (MALDI-TOF): *m*/*z* 2094.9870 [M^+, 100%]; Anal. Calcd for $C_{126}H_{196}O_8S_8$: C, 72.22; H, 9.43; Found: C, 72.41; H, 9.48.

4.3.2. Compound ***1b***. Orange powder, yield: 43%. ^1H NMR ($CDCl_3$, 300 MHz): δ 0.68–2.33 (180H, d, *J* 7.4 Hz, aliphatic and cholesteric protons are overlapped), 2.45 (8H, t, *J* 7.0 Hz, $COCH_2$), 2.90 (8H, t, *J* 7.0 Hz, SCH_2), 4.56–4.74 (4H, m, OCH), 5.6–5.40 (4H, m, =CH). ^{13}C NMR ($CDCl_3$, 75 MHz): δ 11.87, 18.73, 19.35, 21.05, 22.57, 22.82, 23.88, 24.30, 27.84, 28.01, 28.24, 29.15, 31.91, 35.06, 35.80, 36.20, 36.59, 37.01, 38.17, 39.52, 39.75, 42.31, 50.03, 56.17, 56.69, 73.95, 122.67, 127.72, 139.61, 172.55. FT-IR (KBr, cm^{-1}): 2945 (C–H), 1732 (C=O), 1173 (C–O). MS (MALDI-TOF): *m*/*z* 2151.6575 [M^+, 100%]. Anal. Calcd for $C_{130}H_{204}O_8S_8$: C, 72.57; H, 9.56; Found: C, 72.50; H, 9.29.

4.3.3. Compound ***1c***. Orange powder, yield: 42%. ^1H NMR ($CDCl_3$, 300 MHz): δ 0.69–2.33 (196H, m, aliphatic and cholesteric protons are overlapped), 2.84 (8H, t, *J* 7.1 Hz, SCH_2), 4.62 (4H, br s, OCH), 5.37–5.40 (4H, br, =CH). ^{13}C NMR ($CDCl_3$, 75 MHz): δ 11.86, 18.73, 19.35, 21.05, 22.56, 22.81, 23.87, 24.30, 25.00, 27.83, 28.01, 28.24, 30.91, 32.94, 35.54, 35.81, 36.20, 37.00, 38.16, 39.52, 39.74, 42.32, 50.03, 56.18, 56.70, 74.14, 122.70, 127.99, 139.59, 172.06. FT-IR (KBr, cm^{-1}): 2945 (C–H), 1732 (C=O), 1171 (C–O). MS (MALDI-TOF): *m*/*z* 2207.1143[M^+, 100%]. Anal. Calcd for $C_{134}H_{212}O_8S_8$: C, 72.90; H, 9.68; Found: C, 72.59; H, 9.55.

4.3.4. Compound ***1d***. Orange powder, yield: 41%. ^1H NMR ($CDCl_3$, 300 MHz): δ 0.68–2.32 (204H, m, aliphatic and cholesteric protons are overlapped), 2.81 (8H, t, *J* 7.0 Hz, SCH_2), 4.60–4.68 (4H, m, OCH), 5.36–5.39 (4H, br, =CH). ^{13}C NMR ($CDCl_3$, 75 MHz): δ 11.86, 18.72, 19.34, 21.04, 22.57, 22.82, 23.86, 24.51, 27.84, 28.01, 28.32, 28.97, 29.37, 31.90, 35.81, 36.19, 28.17, 39.52, 39.74, 42.32, 50.03, 56.16, 56.69, 73.83, 122.63, 127.70, 139.67, 172.86. FT-IR (KBr, cm^{-1}): 2936 (C–H), 1732 (C=O), 1171 (C–O). MS (MALDI-TOF): *m*/*z* 2261.5801 [M^+, 100%]. Anal. Calcd for $C_{138}H_{220}O_8S_8$: C, 73.52; H, 9.80; Found: C, 73.83; H, 9.89.

4.3.5. Compound ***1e***. Yellow slimy solid, yield: 47%. ^1H NMR ($CDCl_3$, 300 MHz): δ 0.67–2.32 (212H, m, aliphatic and cholesteric protons are overlapped), 2.81 (8H, t, *J* 7.2 Hz, SCH_2), 4.45–4.68 (4H, m, OCH), 5.36–5.39 (4H, m, =CH). ^{13}C NMR (75 MHz, $CDCl_3$): δ 11.86, 18.73, 19.33, 21.04, 22.57, 22.86, 23.86, 24.29, 24.86, 27.84, 27.99, 28.11,

28.23, 28.58, 29.49, 34.53, 35.79, 36.13, 36.20, 36.59, 37.02, 38.18, 39.52, 39.75, 42.31, 50.04, 56.17, 56.69, 73.73, 122.58, 127.71,139.66, 172.94. FT-IR (KBr, cm^{-1}): 2936 (C–H), 1734 (C=O), 1170 (C–O). MS (MALDI-TOF): m/z 2318.6682[M^+, 100%]. Anal. Calcd for $C_{142}H_{228}O_8S_8$: C, 73.52; H, 9.91. Found: C, 73.88; H, 9.97.

Acknowledgements

This work was supported by the National Science Foundation of China (No. 21062022), the Specialized Research Fund for the Doctoral Program of Higher Education (Grant No. 20060184001) and the Open Project of the State Key Laboratory of Supramolecular Structure and Materials.

Supplementary data

Partial experimental details including DSC traces, POM textures, SAXS patterns, UV spectra, and cyclic voltammograms. Supplementary data related to this article can be found online version, at doi:10.1016/j.tet.2010.11.088.

References and notes

1. Lehn, J.-M. *Science* **2002**, *295*, 2400–2403.
2. Kato, T. *Science* **2002**, *295*, 2414–2418.
3. Lawrence, D. S.; Jiang, T.; Levett, M. *Chem. Rev.* **1995**, *95*, 2229–2260.
4. Mallia, V. A.; Tamaoki, N. *Chem. Soc. Rev.* **2004**, *33*, 76–84.
5. *Handbook of Liquid Crystals*; Demus, D., Goodby, J., Gray, G. W., Spiess, H. W., Vill, V., Eds.; Wiley-VCH: Weinheim, 1998; Vols. 1–4.
6. Goodby, J. Liquid Crystals (theme issue), *Chem. Soc. Rev.* **2007**, *36*, 1845–2128.
7. Goodby, J. W.; Saez, I. M.; Cowling, S. J.; Gortz, V.; Draper, M.; Hall, A. W.; Sia, S.; Cosquer, G.; Lee, S.-E.; Raynes, E. P. *Angew. Chem., Int. Ed.* **2008**, *47*, 2754–2787.
8. Bryce, M. R. *Chem. Soc. Rev.* **1991**, *20*, 355–390.
9. Bryce, M. R. *J. Mater. Chem.* **1995**, *5*, 1481–1496.
10. Andreu, R.; Barberá, J.; Garín, J.; Orduna, J.; Serrano, J. L.; Sierra, T.; Leriche, P.; Sallé, M.; Riou, A.; Jubault, M.; Gorgues, A. *J. Mater. Chem.* **1998**, *8*, 881–887.
11. Chen, H. P.; Katsis, D.; Mastrangelo, J. C.; Chen, S. H.; Jacobs, S. D. *Adv. Mater.* **2000**, *12*, 1283–1286.
12. Katsuhara, M.; Aoyagi, I.; Nakajima, H.; Mori, T.; Kambayashi, T.; Ofuji, M.; Takanishi, Y.; Ishikawa, K.; Takezoe, H.; Hosono, H. *Synth. Met.* **2005**, *149*, 219–223.
13. Gao, X.; Wu, W.; Liu, Y.; Jiao, S.; Qiu, W.; Yu, G.; Wang, L.; Zhu, D. *J. Mater. Chem.* **2007**, *17*, 736–743.
14. Bissell, R. A.; Boden, N.; Bushby, R. J.; Fishwick, C. W. G.; Holland, E.; Movaghar, B.; Bushby, R. J.; Ungar, G. *Chem. Commun.* **1998**, 113–114.
15. González, A.; Segura, J. L.; Martín, N. *Tetrahedron Lett.* **2000**, *41*, 3083–3086.
16. Andreu, R.; Garín, J.; Orduna, J.; Barberá, J.; Serrano, J. L.; Sierra, T.; Sallé, M.; Gorgues, A. *Tetrahedron* **1998**, *54*, 3895–3912.
17. Wang, L.; Jeong, K.-U.; Lee, M.-H. *J. Mater. Chem.* **2008**, *18*, 2657–2659.
18. Pintre, I. C.; Serrano, J. L.; Blanca, M.; Folcia, C. L.; Etxebarria, J.; Goc, F.; Amabilino, D. B.; Puigmartí-Luis, J.; Gomar-Nadald, E. *Chem. Commun.* **2008**, 2523–2525.
19. Martínez-Perdiguero, J.; Alonso, I.; Ortega, J.; Folcia, C. L.; Etxebarria, J.; Pintre, I.; Ros, M. B.; Amabilino, D. B. *Phys. Rev. E* **2008**, *77*, 0202701–0202704.
20. Alonso, I.; Martínez-Perdiguero, J.; Folcia, C. L.; Etxebarria, J.; Ortega, J.; Pintre, I. C.; Ros, M. B. *Physical Review E* **2008**, *78*, 041701–041707.
21. Cook, M. J.; Cooke, G.; Jafari-Fini, A. *Chem. Commun.* **1996**, 1925–1926.
22. Borisch, K.; Diele, S.; Göring, P.; Kresse, H.; Tschierske, C. *J. Mater. Chem.* **1998**, *8*, 529–543.
23. Hasimoto, M.; Ujiie, S.; Mori, A. *Adv. Mater.* **2003**, *15*, 797–800.
24. Lee, M.; Yoo, Y. *J. Mater. Chem.* **2002**, *12*, 2161–2168.
25. Poulsen, T.; Nielsen, K. A.; Andrew, D.; Bond, A. D.; Jeppesen, J. O. *Org. Lett.* **2007**, *9*, 5485–5488.
26. Sly, J.; Kasák, P.; Gomar-Nadal, E.; Rovira, C.; Górriz, L.; Thordarson, P.; Amabilino, D. B.; Rowan, A. E.; Nolte, R. J. M. *Chem. Commun.* **2005**, 1255–1257.
27. Hou, R.; Jin, L.; Yin, B. *Inorg. Chem. Commun.* **2009**, *12*, 739–743.
28. Spanggaard, H.; Prehn, J.; Nielsen, M. B.; Levillain, E.; Allain, M.; Becher, J. *J. Am. Chem. Soc.* **2000**, *122*, 9486–9494.
29. Wang, C. S.; Batsanov, A. S.; Bryce, M. R.; Howard, J. A. K. *Synthesis* **1998**, *11*, 1615–1618.
30. Marcelis, A. T. M.; Koudijs, A.; Sudhölter, E. J. R. *Liq. Cryst.* **1995**, *18*, 843–850.